9-1-2013

Moving Objects in the Hubble Ultra Deep Field

Mukremin Kilic
University of Oklahoma, kilic@ou.edu

Alexandros Gianninas
University of Oklahoma, alexg@nhn.ou.edu

Ted von Hippel
Embry-Riddle Aeronautical University, vonhippt@erau.edu

The Astrophysical Journal, 774:88 (11pp), 2013 September 1 doi:10.1088/0004-637X/774/1/88

MOVING OBJECTS IN THE HUBBLE ULTRA DEEP FIELD*

Mukremin Kilic[1], Alexandros Gianninas[1], and Ted von Hippel[2]
[1] Homer L. Dodge Department of Physics and Astronomy, University of Oklahoma, 440 W. Brooks St., Norman, OK 73019, USA; kilic@ou.edu, alexg@nhn.ou.edu
[2] Embry-Riddle Aeronautical University, 600 S. Clyde Morris Blvd., Daytona Beach, FL 32114, USA; ted.vonhippel@erau.edu
Received 2013 May 3; accepted 2013 July 17; published 2013 August 19

ABSTRACT

We identify proper motion objects in the Hubble Ultra Deep Field (UDF) using the optical data from the original UDF program in 2004 and the near-infrared data from the 128 orbit UDF 2012 campaign. There are 12 sources brighter than $I = 27$ mag that display $>3\sigma$ significant proper motions. We do not find any proper motion objects fainter than this magnitude limit. Combining optical and near-infrared photometry, we model the spectral energy distribution of each point-source using stellar templates and state-of-the-art white dwarf models. For $I \leqslant 27$ mag, we identify 23 stars with K0–M6 spectral types and two faint blue objects that are clearly old, thick disk white dwarfs. We measure a thick disk white dwarf space density of 0.1–1.7 $\times$ 10^{-3} pc^{-3} from these two objects. There are no halo white dwarfs in the UDF down to $I = 27$ mag. Combining the Hubble Deep Field North, South, and the UDF data, we do not see any evidence for dark matter in the form of faint halo white dwarfs, and the observed population of white dwarfs can be explained with the standard Galactic models.

Key words: Galaxy: halo – Galaxy: stellar content – Galaxy: structure – proper motions – stars: Population II – white dwarfs

Online-only material: color figures

1. INTRODUCTION

The deepest image of the universe acquired with the *Hubble Space Telescope* (*HST*), the Hubble Ultra Deep Field (UDF; Beckwith 2005), provides a new opportunity to study the structure of the Galactic disk and the halo to its limits. Previously, Ibata et al. (1999) and Méndez & Minniti (2000) used the Hubble Deep Field North (Williams et al. 1996) and South (Casertano et al. 2000) data to constrain the stellar content of the Galaxy. They proposed that the faint blue objects observed in these fields are old halo white dwarfs that would be consistent with the observed microlensing events toward the Large Magellanic Cloud (Alcock et al. 2000; Calchi Novati 2010) and would explain part of the dark matter in the solar neighborhood. Kilic et al. (2004, 2005), Pirzkal et al. (2005), and Mahmud & Anderson (2008) showed that some of these faint blue objects are confused with quasars and an extensive study including proper motion measurements and spectral energy distribution (SED) fitting is required to identify stars in deep *HST* images.

The UDF is the only deep field that is studied spectroscopically by the pioneering work of Pirzkal et al. (2005). Using the Advanced Camera for Surveys (ACS) observations of the UDF and the low resolution spectroscopy from the Grism ACS program for Extragalactic Science survey (GRAPES; Pirzkal et al. 2004), Pirzkal et al. (2005) identified 26 stars and 2 quasars brighter than $I = 27$ mag and additional 18 unresolved sources with 27 mag $< I <$ 29.5 mag. They defined a stellarity index (S_i) using the curve of growth analysis of the light distribution of each object, and identified all objects with $S_i \leqslant 0.05$ as unresolved sources. More importantly, the GRAPES spectra enabled Pirzkal et al. (2005) to differentiate blue extragalactic objects, i.e., quasars, from stars down to fainter magnitudes. They spectroscopically confirmed 2 of the 18 faint unresolved sources as quasars, and classified the remaining 16 sources as stars. Assuming that these objects are main-sequence stars, they would have to be at distances larger than 300 kpc. Therefore, the only viable explanation for these objects would be faint white dwarfs in the thick disk or halo of the Galaxy. If these are high-velocity white dwarfs, they could contribute <10% to the total dark matter halo mass. On the other hand, not all of these sources are expected to be stars and some contamination from blue extragalactic sources is likely.

Pirzkal et al. (2005) split the UDF data set into two halves with a baseline of 73 days, and demonstrated that there are no sources with proper motion $\mu \geqslant 27$ mas yr^{-1}. Mahmud & Anderson (2008) used shallower data from two additional epochs with a 3 yr baseline to identify proper motion objects, finding seven objects with significant proper motions.

Here we take advantage of the Wide Field Camera 3 infrared data from the UDF12 campaign, a 128 orbit large *HST* program (Ellis et al. 2013; Koekemoer et al. 2012), to measure proper motions for the point sources identified by Pirzkal et al. (2005), including sources fainter than $I = 27$ mag. These data were obtained in 2012 August–September, and provide an ≈8.7 yr baseline for astrometry. Koekemoer et al. (2012) describe data reduction and calibration procedures for these observations. The UDF12 observations in four near-infrared filters, F105W, F125W, F140W, and F160W, also greatly extend our ability to constrain the spectral type for each object. The deepest images are in the F105W (100 orbits) and F160W (84 orbits) bands, which correspond roughly to J and H filters, respectively. The 5σ limiting sensitivity of the F105W image reaches an AB magnitude of 30. Hence, these data provide the best opportunity yet to measure proper motions and to model the SEDs of the stars in the UDF.

Section 2 describes the identification of point sources, while Section 3 presents our proper motion measurements. Section 4 describes our SED fitting procedures and classifications for the faint sources in the UDF. We discuss various implications of these results in Section 5.

* Based on observations made with the NASA/ESA *Hubble Space Telescope*, obtained from the Data Archive at the Space Telescope Science Institute, which is operated by the Association of Universities for Research in Astronomy, Inc., under NASA contract NAS 5-26555.

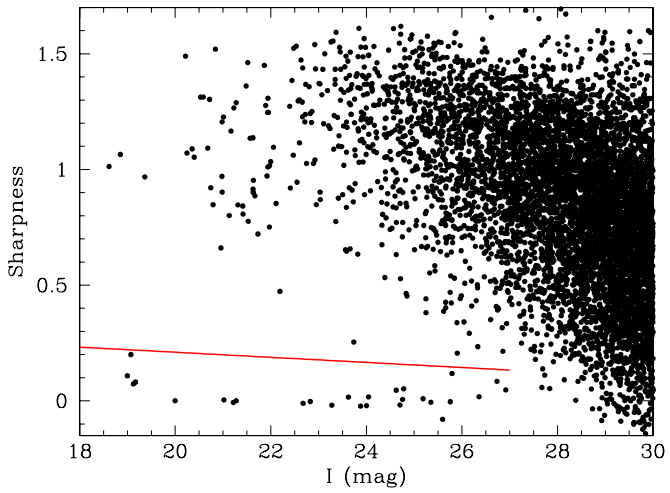

Figure 1. Distribution of the sharpness parameter from DAOPHOT for the UDF objects. Objects below the solid line are unresolved.

(A color version of this figure is available in the online journal.)

2. IDENTIFICATION OF POINT SOURCES

To identify unresolved sources, Pirzkal et al. (2005) used the IRAF task RADPROF and performed aperture photometry using increasing aperture sizes. They fit a cubic spline to these measurements to create a point-spread function (PSF) for each object. They compared each PSF with the empirical combined-PSF from bright unresolved objects, and classified objects with PSF distributions similar to this empirical PSF as unresolved sources. This approach works well for bright targets, but it is likely to fail for nearly unresolved faint objects. The discovery of 16 unresolved sources with $I \geqslant 27$ mag in the UDF is potentially important, but clearly unexpected.

To verify the classification of point sources and to derive precise centroids for each target, we use the IRAF DAOPHOT package to create a PSF template using bright, unsaturated, isolated targets in the I-band (deepest) image and use this template to fit each object. Figure 1 shows the sharpness parameter (S_I) derived from DAOPHOT as a function of magnitude. Stars have $S_I \approx 0$, whereas resolved objects have increasingly larger S_I based on their morphology. This figure demonstrates that the point sources can be identified reliably down to about $I = 27$ mag. Pirzkal et al. (2005) identified 28 point sources, including two spectroscopically confirmed quasars, brighter than $I = 27$ mag. All but one of these sources, UDF 4322, have S_I indicative of stars.

Figure 2 presents the PSF distributions for 23 of these 28 sources that are not saturated in the I-band image. S_I for each source is also given in each panel. We use the IRAF task PRADPROF to plot the radial profile of each object. We also plot the I-band PSF template in each panel for a direct comparison. A comparison of the PSF for each object with our template PSF shows that all but one of these sources have PSF distributions consistent with being unresolved. The PSF distribution for UDF 4322 is slightly shallower than the other

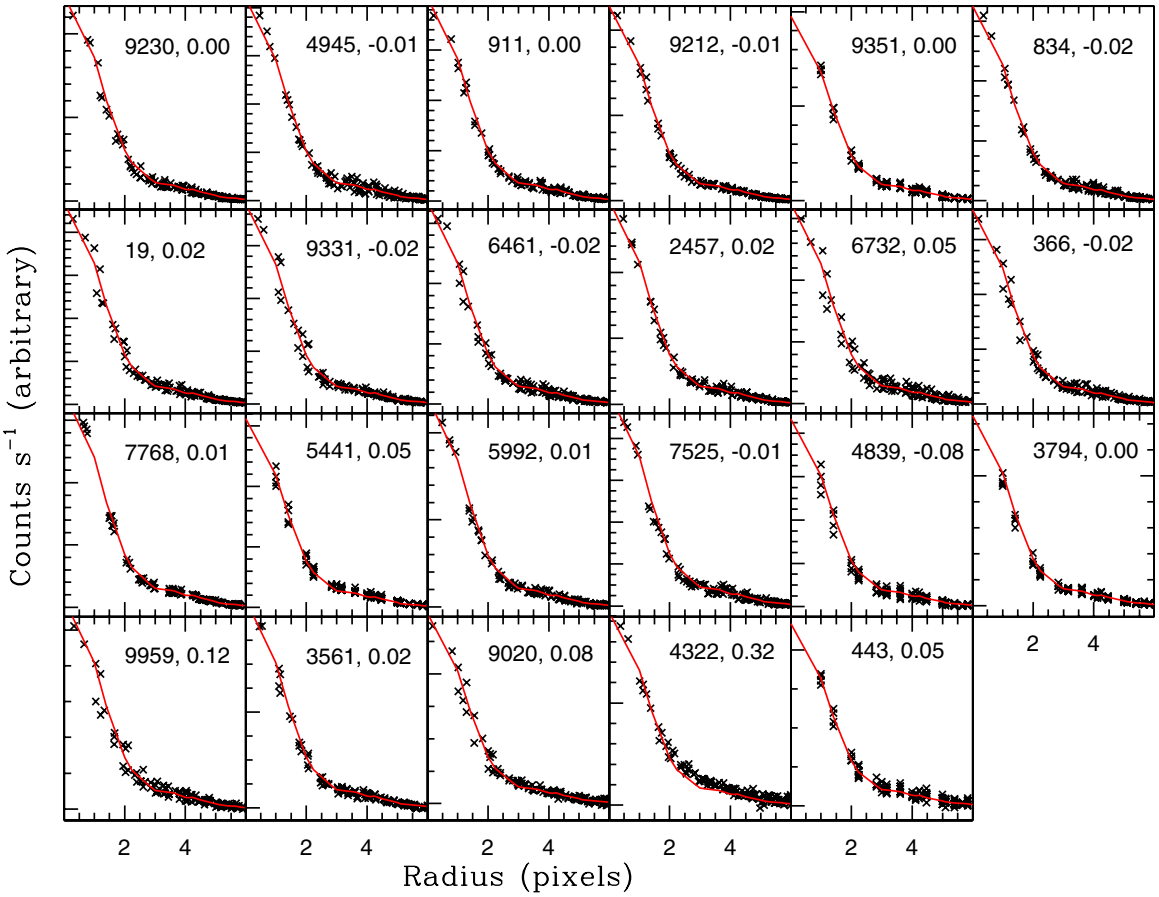

Figure 2. Radial profiles of the relatively bright ($I < 27$ mag), unsaturated, and unresolved source candidates identified by Pirzkal et al. (2005). The objects are shown in increasing I-band magnitude (from top left to bottom right). The PSF template derived from bright isolated stars (solid line) is shown in each panel for comparison. The sharpness parameter for each object is also given after the object name. UDF 4322 has a shallower profile compared to the PSF template and is likely resolved.

(A color version of this figure is available in the online journal.)

point sources, and UDF 4322 is likely a resolved object. All of the unresolved objects in the UDF, except saturated sources, have $S_I \leqslant 0.12$, while UDF 4322 has $S_I = 0.32$. We note that UDF 4322 also has an SED significantly different from the stellar objects (see Section 4).

Figure 3 presents the contour maps of the flux distribution around UDF 4322 and an unresolved source with a similar brightness. A comparison of the contour maps for UDF 4322 ($I = 26.84$ mag) with UDF 443 ($I = 26.92$ mag) shows that unresolved sources have circular contour maps, whereas UDF 4322 is elongated, and slightly resolved in the I band image. Excluding UDF 4322 from the list of unresolved objects and the two spectroscopically confirmed quasars (UDF 6732 and 9397), there are 25 sources brighter than $I = 27$ mag that are clearly stellar.

The morphological classification of point sources is more problematic for fainter magnitudes. Pirzkal et al. (2005) classify 18 objects with $I \geqslant 27$ mag as point sources, including two quasars (UDF 4120 and 8157). Figure 4 presents the PSF distributions of these 18 sources compared to the I-band PSF template derived from brighter stellar sources. It is clear from this figure that the majority of these fainter sources are likely resolved objects. Only two of these sources, UDF 7113 and 8081, have radial profiles consistent with unresolved objects and $S_I \approx 0$. The radial profiles for the remaining 16 targets are too shallow to be stellar.

3. PROPER MOTION MEASUREMENTS

Proper motion measurements are the best way to identify stars in deep *HST* images, and to distinguish between unresolved quasars and stellar objects. They are also crucial for constraining the kinematic properties of each object, and assigning membership in the Galactic disk or halo.

To identify high proper motion objects in the UDF, we used the deepest images from the UDF 2004 and UDF12 datasets; I(F775W)-, J(F105W)-, and H(F160W)-band images. Beckwith (2005) provided source catalogs for the first epoch data using the Source Extractor package (Bertin & Arnouts 1996), which is designed to work best for resolved objects. We used the DAOPHOT package to create a PSF template for each filter and used this template to precisely constrain the centroids for each object in each epoch.

We identified >200 compact objects (isolated, low residuals, and not fuzzy) that can be used as reference objects to define an absolute reference frame. These sources have half light radii R50 < 4 pixels, ellipticity <0.5, FWHM <8 pixels, and stellarity index (as defined by Source Extractor) larger than 0.7. We visually inspected all of these sources in different filters to avoid any mismatches. We used the IRAF routine GEOMAP to fit a quadratic polynomial to map the distortions and deleted deviant points using a 3σ rejection algorithm. Rejection of very deviant points is required because the reference objects are compact galaxies and centroiding errors are larger for galaxies. After mapping the distortions with the GEOMAP package, we transformed the object coordinates to the second epoch positions with the GEOXYTRAN routine. Using the reference objects, we confirm the pixel size difference between the optical and infrared images (30 mas versus 60 mas pixel^{-1}) and that their orientations are aligned to better than $0\overset{\circ}{.}002$.

Figure 5 presents the differences in position between the UDF04 I-band and the UDF12 F105W images for 200 compact objects that form our reference frame. Red circles mark objects brighter than $I = 27$ mag. The majority of these compact

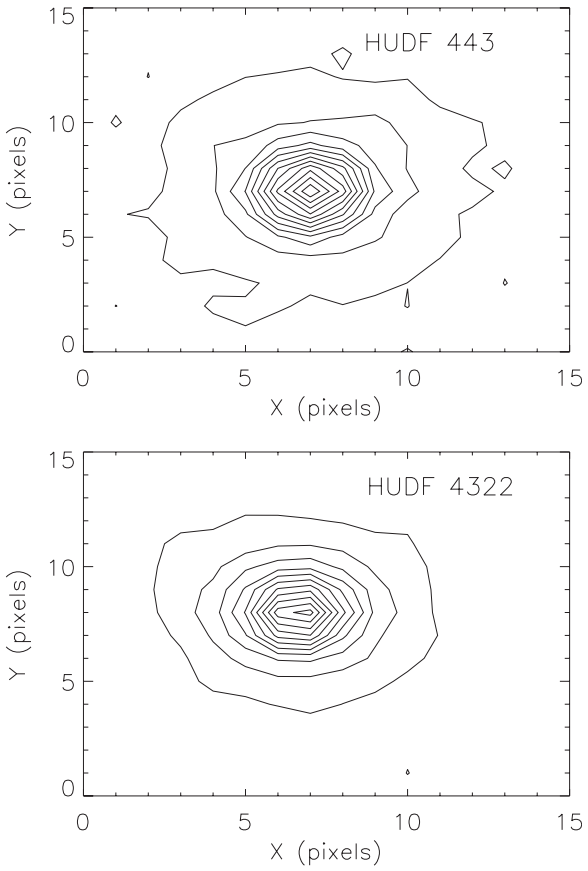

Figure 3. Contour maps of the flux distribution around UDF 443 and 4322 in the I-band.

sources do not show any positional differences over the 8.7 yr baseline. However, there are seven objects brighter than $I = 27$ mag that show significant motion. These sources are labeled in the figure and they are clearly stars. We check these results using our second deepest image in the UDF12 dataset, the F160W image. The dotted lines mark the location of each source in the F160W image. Since the F160W image mostly consists of the data from the UDF09 program, the baseline between the I and F160W images are shorter. The observed locations of the seven moving objects in the F160W image are consistent with the F105W image positions, providing further evidence that these seven relatively bright objects are clearly moving.

There are several fainter objects with $I > 27$ mag that show significant motion in the F105W image. However, none of these objects show the same motion in the F160W image, indicating that they are likely resolved galaxies. Color-dependent morphological differences in these galaxies may cause our PSF-fitting algorithm to find slightly different centroids for these faint sources, and explain the differences in positions measured from the I-band, F105W, and F160W images. Hence, we do not find any moving objects fainter than $I = 27$ mag.

The main source of error in our proper motion measurements is the positions of the reference compact objects (galaxies). The residuals in the coordinate transformations are 0.3 pixels (9 mas) in each coordinate. Given the 8.7 yr baseline between the UDF04 and UDF12 programs, this corresponds to 1.04 mas yr^{-1} errors in each coordinate, or 1.47 mas yr^{-1} total proper motion errors for each source. Tables 1 and 2 present the proper motions for 46 unresolved source candidates identified by Pirzkal et al. (2005). The near-infrared images from the Wide Field Camera 3 cover an area smaller than the optical data. Hence, some of these

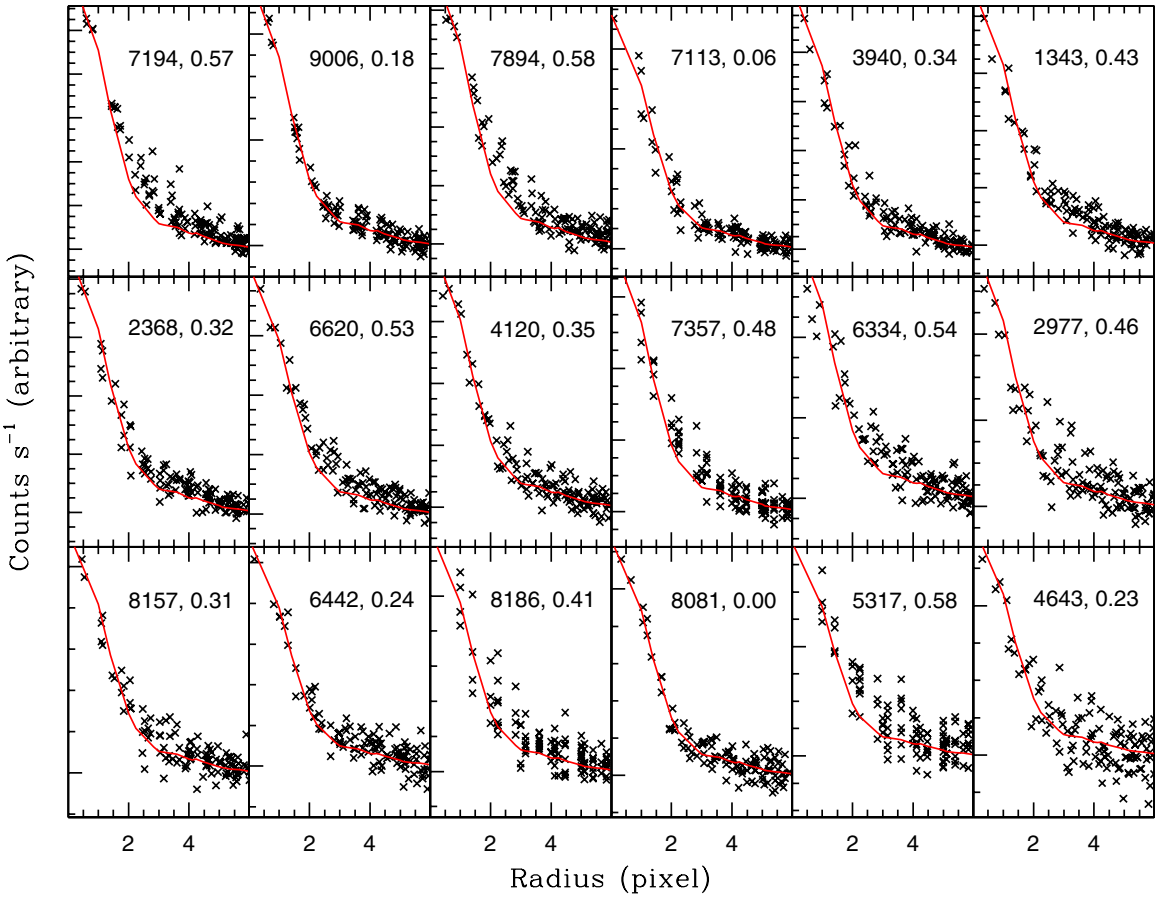

Figure 4. Similar to Figure 2, but for faint ($I > 27$ mag) unresolved source candidates. UDF 7113 and 8081 are the only faint objects with sharpness ≈0 and radial profiles consistent with unresolved sources.

(A color version of this figure is available in the online journal.)

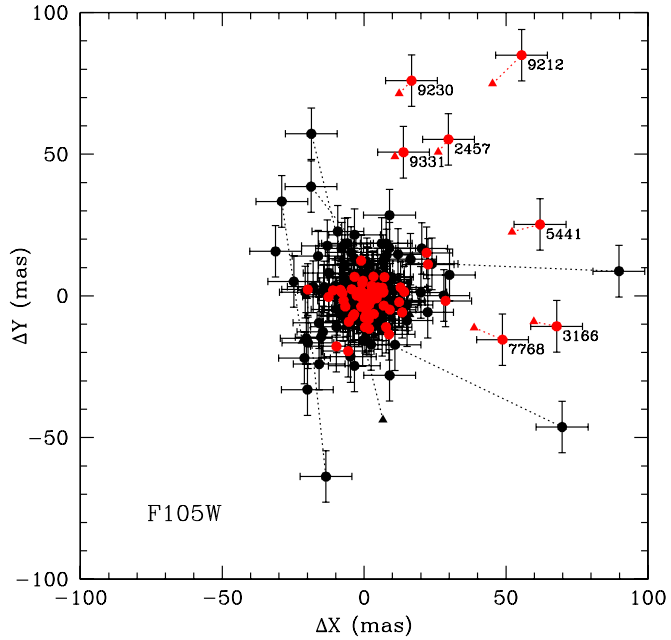

Figure 5. Differences in positions for 200 compact UDF sources between the 2004 *I*-band and 2012 F105W images (circles). Triangles represent the positions of the same sources in the F160W image. The dotted lines connect the astrometric data derived from the F105W and F160W filters. Objects brighter than $I = 27$ mag are marked by red points and the objects with significant motion are labeled.

(A color version of this figure is available in the online journal.)

sources are not in the UDF12 dataset. On the other hand, a few of the brighter sources have proper motion measurements from an earlier epoch (Mahmud & Anderson 2008). We include these measurements in Table 1 to have a nearly complete list of proper motions for each source. In total, there are 12 sources with ($>3\sigma$) significant proper motions.

Figure 6 compares proper motion measurements for 11 objects that are common between our study and that of Mahmud & Anderson (2008). The latter study is limited to $I < 27$ mag objects due to shallower data. Our measurements agree with the Mahmud & Anderson (2008) results within 1σ errors. This gives us confidence that our proper motion measurements are reliable.

4. SPECTRAL TYPES OF STARS IN THE UDF

4.1. Bright ($I < 27$ mag) Unresolved Sources

Pirzkal et al. (2005) determined the spectral types of the unresolved objects in the UDF by fitting stellar templates to the low resolution grism spectroscopy from the GRAPES survey. The spectroscopic data quality degrades with increasing magnitude and the background subtraction becomes the limiting factor for the objects fainter than $I = 27$ mag. The SEDs for the majority of the unresolved sources are best-fit with late-type K–M stars, where infrared data would be extremely useful, but was unavailable for the initial analysis by Pirzkal et al. (2005) and Mahmud & Anderson (2008).

Table 1
Physical Properties of the Bright ($I < 27$ mag) Unresolved Sources

Object	μ (mas yr^{-1})	μ_{2008} (mas yr^{-1})	Spectral Type	M_{F606W} (mag)	d (kpc)	V_{tan} (km s^{-1})	T_{eff_0} (K)	T_{eff_2} (K)
19	...	...	M1	8.7	15	...	3800	3400
366	...	2.42 ± 1.47	M6	13.6	7	80	2300	2000
443	...	...	M6	13.6	19	...	2200	2000
834	...	0.27 ± 0.96	M5	12.2	4	10	2900	2700
911	...	27.01 ± 0.78	M4	11.1	3	320	3100	2800
1147	...	5.49 ± 0.63	K3	6.6	4	110	4800	4900
2150	...	25.16 ± 0.45	M3	10.2	1	140	3200	2900
2457	7.25 ± 1.47	7.87 ± 0.82	M0	8.3	22	750	3900	3500
3166	7.94 ± 1.47	8.84 ± 0.66	K7	7.9	2	90	4000	3700
3561	2.90 ± 1.47	...	M0	8.3	62	850	3900	3600
3794	3.09 ± 1.47	4.90 ± 2.75	M1	8.7	41	590	3900	3500
4322	...	...	A7	2.1	877	...	7600	7600
4839	...	11.64 ± 1.92	K2	6.0	100	5530	4800	4800
4945	...	...	M4	11.1	2	...	3100	2800
5441	7.74 ± 1.47	8.35 ± 1.14	M2	9.2	24	860	3600	3200
5921	...	3.27 ± 1.26	K7	7.9	2	40	4100	3800
5992	1.64 ± 1.47	1.18 ± 1.71	K7	7.9	40	310	4200	4000
6461	...	...	M0	8.3	22	...	3900	3500
6732	0.13 ± 1.47	0.42 ± 1.14	QSO	...	...	...	...	...
7525	...	4.10 ± 1.50	M1	8.7	35	680	3800	3400
7768	5.92 ± 1.47	6.50 ± 1.14	K7	7.9	32	910	4200	4000
9020	3.33 ± 1.47	...	F5	3.5	443	6980	6800	7000
9212	11.73 ± 1.47	12.35 ± 0.54	M0	8.3	12	650	3900	3500
9230	8.99 ± 1.47	10.26 ± 0.41	K0	5.4	10	420	4900	5000
9331	6.08 ± 1.47	6.39 ± 0.73	M4	11.1	8	240	3000	2800
9351	...	12.11 ± 0.68	M2.5	9.7	8	440	3500	3100
9397	0.47 ± 1.47	0.70 ± 0.47	QSO	...	...	...	...	...
9959	...	...	M0	8.3	47	...	4000	3600

Notes. μ and μ_{2008} are proper motions from this study and Mahmud & Anderson (2008), respectively. T_{eff_0} and T_{eff_2} are the temperatures of the best-fit PHOENIX models with [Fe/H] = 0 and [Fe/H] = −2, respectively.

Table 2
Proper Motion Measurements for the Faint ($I > 27$ mag) Unresolved Sources

Object	μ (mas yr^{-1})
1343	...
2368	2.11
2977	...
3940	0.18
4120	...
4643	...
5317	...
6334	1.25
6442	1.01
6620	0.33
7113	0.58
7194	0.65
7357	0.44
7894	0.29
8081	2.36
8157	0.56
8186	...
9006	0.36

Notes. UDF 4120 and 8157 are spectroscopically confirmed quasars. All proper motion measurements are from this study and have errors of 1.47 mas yr^{-1}.

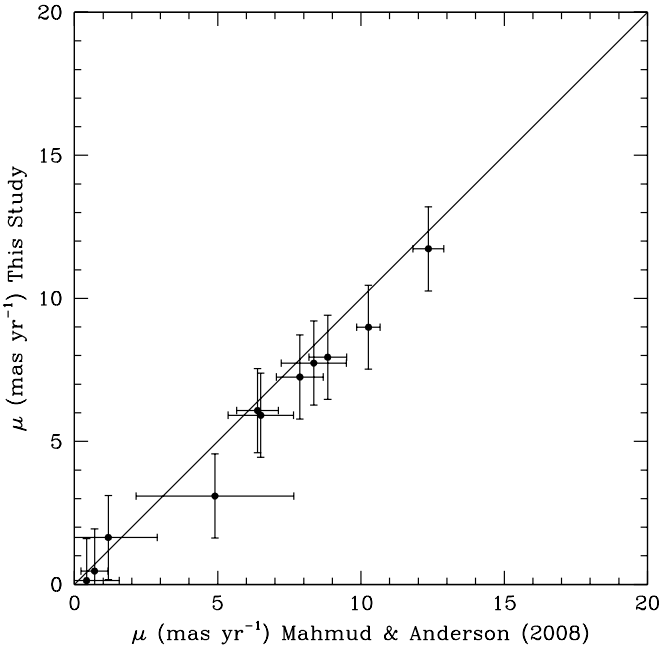

Figure 6. Comparison between proper motion measurements for 11 objects that are common between this study and Mahmud & Anderson (2008). The results agree within 1σ errors.

Using the F105W, F125W, F140W, and F160W data in the UDF12 program, we perform PSF-photometry for the unresolved sources detected in these images. We use an aperture size of 0.″4 and AB magnitude zeropoints of 26.0974, 26.0449, 26.2608, and 25.7551 for the F105W, F125W, F140W, and F160W images, respectively. In addition, a few of the targets outside the field-of-view of the UDF12 observations have infrared photometry available from NICMOS observations in the F110W and F160W filters (Coe et al. 2006). Table 3

Table 3
Optical and Infrared Photometry (in the AB System) for the Unresolved Source Candidates in the UDF

Object	F435W	F606W	F775W	F850LP	F105W	F125W	F140W	F160W	F110W	F160W
19	26.563 ± 0.030	24.643 ± 0.004	23.626 ± 0.002	23.309 ± 0.002	...	...	...	...	...	...
366	30.731 ± 1.018	27.723 ± 0.044	24.704 ± 0.003	23.423 ± 0.002	...	...	...	...	...	...
443	...	29.973 ± 0.200	26.917 ± 0.014	25.448 ± 0.006	...	...	...	...	...	...
834	27.416 ± 0.079	25.252 ± 0.008	23.277 ± 0.001	22.496 ± 0.001	...	...	...	...	22.061 ± 0.072	22.029 ± 0.082
911	25.047 ± 0.017	23.053 ± 0.002	21.275 ± 0.000	20.607 ± 0.000	...	...	...	...	...	...
1147	19.530 ± 0.000	19.662 ± 0.000	19.168 ± 0.000	19.040 ± 0.000	...	...	...	...	...	...
1343	27.455 ± 0.027	27.655 ± 0.021	27.791 ± 0.027	27.903 ± 0.052	...	...	...	...	...	...
2150	22.535 ± 0.003	20.558 ± 0.000	19.126 ± 0.000	18.320 ± 0.000	...	...	...	...	18.266 ± 0.052	18.024 ± 0.064
2368	29.250 ± 0.128	27.961 ± 0.027	27.805 ± 0.026	27.972 ± 0.053	27.922 ± 0.049	28.004 ± 0.064	28.071 ± 0.036	28.031 ± 0.060	27.920 ± 0.317	27.522 ± 0.294
2457	26.793 ± 0.036	25.004 ± 0.005	24.047 ± 0.002	23.733 ± 0.003	23.521 ± 0.012	23.377 ± 0.018	23.336 ± 0.012	23.303 ± 0.007	23.578 ± 0.086	23.334 ± 0.098
2977	28.024 ± 0.040	28.160 ± 0.032	28.261 ± 0.038	28.196 ± 0.062	...	...	...	...	28.016 ± 0.368	28.070 ± 0.436
3166	20.753 ± 0.001	19.786 ± 0.000	18.998 ± 0.000	18.628 ± 0.000	18.548 ± 0.002	18.438 ± 0.003	18.362 ± 0.001	18.281 ± 0.001	18.697 ± 0.052	18.497 ± 0.064
3561	29.013 ± 0.121	27.263 ± 0.017	26.360 ± 0.008	26.119 ± 0.012	25.745 ± 0.014	25.612 ± 0.008	25.574 ± 0.010	25.570 ± 0.008	25.986 ± 0.134	25.780 ± 0.137
3794	28.869 ± 0.126	26.740 ± 0.013	25.757 ± 0.006	25.477 ± 0.008	25.143 ± 0.011	25.012 ± 0.015	24.996 ± 0.009	24.955 ± 0.008	25.251 ± 0.111	25.232 ± 0.116
3940	27.084 ± 0.017	27.562 ± 0.019	27.704 ± 0.024	27.917 ± 0.051	27.652 ± 0.023	27.599 ± 0.026	27.682 ± 0.021	27.332 ± 0.013	27.319 ± 0.202	26.639 ± 0.166
4120	28.143 ± 0.045	28.046 ± 0.029	27.876 ± 0.028	26.631 ± 0.016	...	...	...	...	27.212 ± 0.229	27.521 ± 0.311
4322	26.856 ± 0.021	26.816 ± 0.014	26.843 ± 0.016	26.913 ± 0.030	...	...	...	...	26.831 ± 0.194	26.017 ± 0.169
4643	32.672 ± 2.017	30.054 ± 0.130	29.259 ± 0.072	29.025 ± 0.102	...	...	...	...	28.710 ± 0.667	99.000 ± 28.498
4839	27.232 ± 0.030	26.007 ± 0.007	25.594 ± 0.005	25.523 ± 0.009	...	...	...	...	25.537 ± 0.125	26.120 ± 0.147
4945	24.752 ± 0.013	22.925 ± 0.002	21.215 ± 0.000	20.536 ± 0.000	...	...	...	...	...	...
5317	28.915 ± 0.078	28.625 ± 0.041	28.584 ± 0.044	28.838 ± 0.097	...	...	...	...	...	...
5441	27.817 ± 0.079	26.052 ± 0.011	24.781 ± 0.004	24.384 ± 0.005	24.040 ± 0.006	23.897 ± 0.007	23.881 ± 0.005	23.867 ± 0.005	24.137 ± 0.094	24.039 ± 0.106
5921	20.520 ± 0.001	19.737 ± 0.000	19.072 ± 0.000	18.571 ± 0.000	...	...	...	...	...	...
5992	27.491 ± 0.041	25.888 ± 0.007	25.186 ± 0.004	25.030 ± 0.006	24.736 ± 0.010	24.637 ± 0.015	24.591 ± 0.013	24.545 ± 0.012	25.023 ± 0.104	24.858 ± 0.115
6334	27.789 ± 0.032	27.983 ± 0.027	28.091 ± 0.032	28.197 ± 0.062	28.010 ± 0.025	27.978 ± 0.039	27.661 ± 0.039	27.575 ± 0.029	27.722 ± 0.382	27.638 ± 0.397
6442	28.158 ± 0.042	28.371 ± 0.036	28.356 ± 0.039	28.382 ± 0.070	27.746 ± 0.022	27.628 ± 0.028	27.894 ± 0.037	27.656 ± 0.024	28.502 ± 0.665	28.375 ± 0.715
6461	26.660 ± 0.033	24.990 ± 0.005	24.003 ± 0.002	23.698 ± 0.003	...	...	...	...	...	...
6620	30.811 ± 0.512	28.119 ± 0.031	27.825 ± 0.026	28.020 ± 0.054	27.650 ± 0.037	27.642 ± 0.027	27.650 ± 0.038	27.505 ± 0.034	...	27.063 ± 0.291
6732	25.706 ± 0.012	24.588 ± 0.003	24.626 ± 0.003	24.606 ± 0.006	23.949 ± 0.020	23.872 ± 0.020	23.685 ± 0.020	23.712 ± 0.022	24.238 ± 0.088	23.992 ± 0.099
7113	30.667 ± 0.518	28.376 ± 0.046	27.673 ± 0.026	27.455 ± 0.037	27.145 ± 0.013	27.064 ± 0.017	26.949 ± 0.013	26.898 ± 0.011	27.016 ± 0.220	26.923 ± 0.231
7194	26.921 ± 0.018	27.050 ± 0.014	27.202 ± 0.018	27.243 ± 0.034	27.109 ± 0.035	26.806 ± 0.034	26.953 ± 0.035	26.977 ± 0.034	...	...
7357	27.984 ± 0.036	27.862 ± 0.023	28.055 ± 0.030	28.288 ± 0.064	28.068 ± 0.021	28.115 ± 0.036	28.081 ± 0.020	28.060 ± 0.032	27.801 ± 0.326	27.624 ± 0.350
7525	28.498 ± 0.113	26.416 ± 0.012	25.350 ± 0.005	25.045 ± 0.007	...	...	...	...	...	...
7768	27.119 ± 0.033	25.444 ± 0.005	24.758 ± 0.003	24.553 ± 0.005	24.278 ± 0.022	24.203 ± 0.021	24.169 ± 0.016	24.196 ± 0.013	...	...
7894	27.531 ± 0.027	27.455 ± 0.018	27.589 ± 0.023	27.794 ± 0.050	27.636 ± 0.031	27.486 ± 0.034	27.503 ± 0.025	27.457 ± 0.031	...	...
8081	27.921 ± 0.032	28.097 ± 0.027	28.382 ± 0.039	28.448 ± 0.072	27.952 ± 0.046	28.163 ± 0.031	27.792 ± 0.037	27.612 ± 0.029	28.022 ± 0.572	28.033 ± 0.668
8157	...	28.728 ± 0.050	28.344 ± 0.039	28.313 ± 0.067	28.310 ± 0.052	28.338 ± 0.069	28.332 ± 0.067	28.353 ± 0.077	28.565 ± 0.524	28.680 ± 0.667
8186	27.974 ± 0.031	28.121 ± 0.025	28.377 ± 0.037	28.646 ± 0.083	...	...	...	...	...	...
9006	27.454 ± 0.025	27.551 ± 0.019	27.538 ± 0.022	27.347 ± 0.032	26.670 ± 0.027	26.727 ± 0.025	27.092 ± 0.032	26.864 ± 0.023	...	...
9020	27.024 ± 0.018	26.731 ± 0.010	26.732 ± 0.011	26.905 ± 0.022	26.741 ± 0.014	26.907 ± 0.018	27.033 ± 0.015	27.123 ± 0.011	26.638 ± 0.170	26.985 ± 0.209
9212	25.494 ± 0.014	23.642 ± 0.002	22.676 ± 0.001	22.373 ± 0.001	22.122 ± 0.012	21.998 ± 0.026	21.971 ± 0.014	21.953 ± 0.014	...	...
9230	21.125 ± 0.001	20.380 ± 0.000	19.999 ± 0.000	19.888 ± 0.000	19.993 ± 0.014	19.953 ± 0.022	19.948 ± 0.025	19.933 ± 0.009	19.866 ± 0.052	19.889 ± 0.064
9331	27.937 ± 0.093	25.706 ± 0.009	23.879 ± 0.002	23.180 ± 0.002	22.746 ± 0.014	22.553 ± 0.023	22.539 ± 0.017	22.536 ± 0.014	23.117 ± 0.086	22.915 ± 0.096
9351	26.101 ± 0.021	24.138 ± 0.003	22.826 ± 0.001	22.386 ± 0.001	...	...	...	...	...	...
9397	21.394 ± 0.001	21.137 ± 0.000	21.020 ± 0.000	20.977 ± 0.001	21.047 ± 0.020	20.940 ± 0.020	20.886 ± 0.020	20.600 ± 0.022	20.738 ± 0.053	20.294 ± 0.064
9959	28.731 ± 0.140	26.676 ± 0.016	25.792 ± 0.008	25.519 ± 0.010	...	...	...	...	...	...

Notes. Optical photometry is from Beckwith (2005) and the last two columns are NICMOS F110W and F160W photometry from Coe et al. (2006).

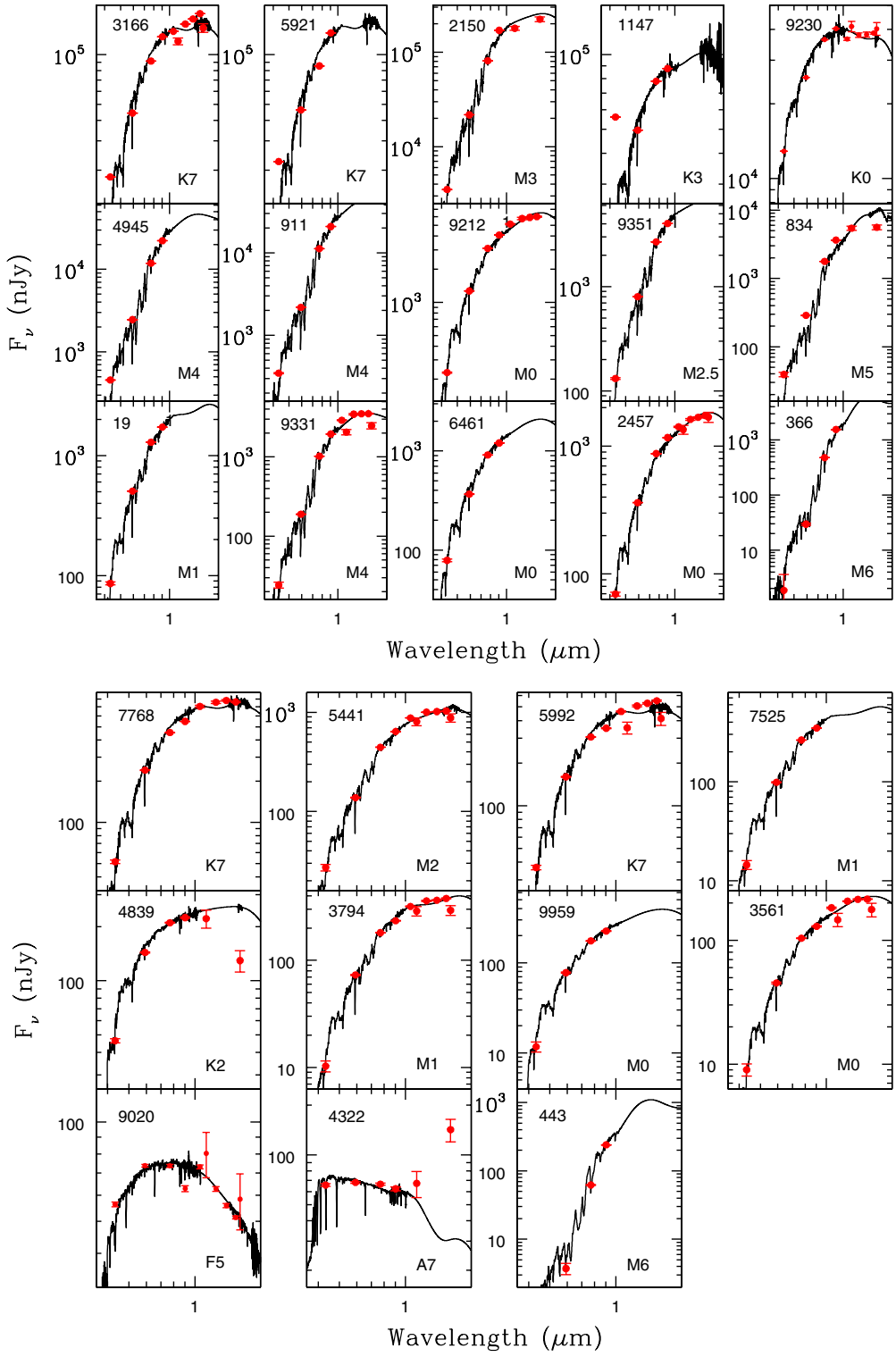

Figure 7. Optical and infrared SEDs and best-fitting main-sequence star templates (Pickles 1998) for the bright ($I < 27$ mag) unresolved source candidates, excluding quasars.

(A color version of this figure is available in the online journal.)

presents all available optical and infrared photometry for the 46 unresolved source candidates.

We attempt to fit the SEDs of the UDF objects by combining *B*, *V*, *I*, and *z* photometry from Beckwith (2005), our own photometry in the F105W, F125W, F140W, and F160W filters, and the NICMOS photometry in the F110W and F160W filters. We use the IRAF task CALCPHOT, which is designed for simulating the *HST* observations, to simulate the SEDs for main-sequence stars using Pickles (1998) stellar templates for O5 to M6 dwarfs. We assign spectral types to each object using a χ^2 minimization technique, where photometry in each band is weighted according to its error.

Figure 7 shows the optical and infrared SEDs and our best-fit templates for the 26 bright ($I < 27$ mag) unresolved source

candidates, excluding the quasars UDF 6732 and 9397. Our classifications for the stars agree reasonably well with the Pirzkal et al. (2005) classifications, but are superior to the previous analysis due to the combination of optical and infrared photometry. One of these sources, UDF 4322, has an optical SED similar to A7 type stars. However, its infrared SED shows a flux excess that is similar to the spectroscopically confirmed quasars in the UDF. Hence, based on its morphology (Figures 2 and 3) and optical and infrared SED, UDF 4322 is most likely an extragalactic object.

The SEDs for the remaining 25 targets fit spectral templates fairly well. We identify 17 M dwarfs, 7 K dwarfs, and 1 F type star (UDF 9020), which is certainly a white dwarf (see the discussion below). In addition, UDF 4839 has optical photometry that is consistent with a K2 dwarf, but its infrared photometry is significantly fainter than expected for K dwarfs. This star must be a white dwarf as well.

One of our targets, UDF 1147, is the brightest object in the B filter and overly saturated in that image. Its spectrum implies a ~F7 type star, though its VIz photometry is more consistent with a K3 dwarf star. Therefore, we conclude that either its B photometry is wrong, or it may have a hotter companion. Unfortunately, the GRAPES spectrum does not go blue enough to confirm this result, but the blue excess is apparent in its photometry with $B - V = -0.13$ and $V - I = 0.49$ mag.

Pirzkal et al. (2005) identified two L dwarf candidates, UDF 366 and 443. Unfortunately, these objects are not in the field of view of the NICMOS or WFC3 infrared observations. The optical SEDs for these two sources match an M6 spectral template, which is the latest spectral type available in the Pickles (1998) library. Follow-up near-infrared observations will be useful to constrain the spectral types for UDF 366 and 443 more precisely.

4.2. Faint ($I > 27$ mag) Unresolved Sources

Figure 8 shows optical and infrared color–color diagrams for the 46 unresolved source candidates along with the synthetic colors for O5–M6 type stars and cool white dwarfs with pure H and pure He atmospheres (Tremblay & Bergeron 2009; Bergeron et al. 2011). These 46 sources follow the stellar sequence in the optical color–color diagrams (top panel). However, the majority of the faint ($I > 27$ mag) sources and UDF 4322 have infrared colors significantly different than stars (bottom panel). These objects have infrared colors similar to the spectroscopically confirmed quasars UDF 6732 and 9397. Pirzkal et al. (2005) note that some of these faint sources are hard to distinguish from extragalactic sources without higher signal-to-noise ratio spectra or accurate proper-motion measurements. Contamination from the large number of extragalactic objects is inevitable at these faint magnitudes. Our proper motion measurements for these sources (Table 2), their radial profiles (Figure 4), and infrared photometry demonstrate that the majority of the faint unresolved source candidates are extragalactic objects.

Among the 18 faint ($I > 27$ mag) unresolved source candidates, none show significant proper motion (Table 2), 2 are spectroscopically confirmed quasars, and 14 are most likely resolved objects with radial profiles shallower than the template PSF (Figure 4). UDF 7113 and 8081 are the only objects with steep radial profiles similar to the unresolved stellar objects brighter than $I = 27$ mag. Their sharpness parameters from DAOPHOT ($\leqslant 0.06$) are consistent with unresolved sources.

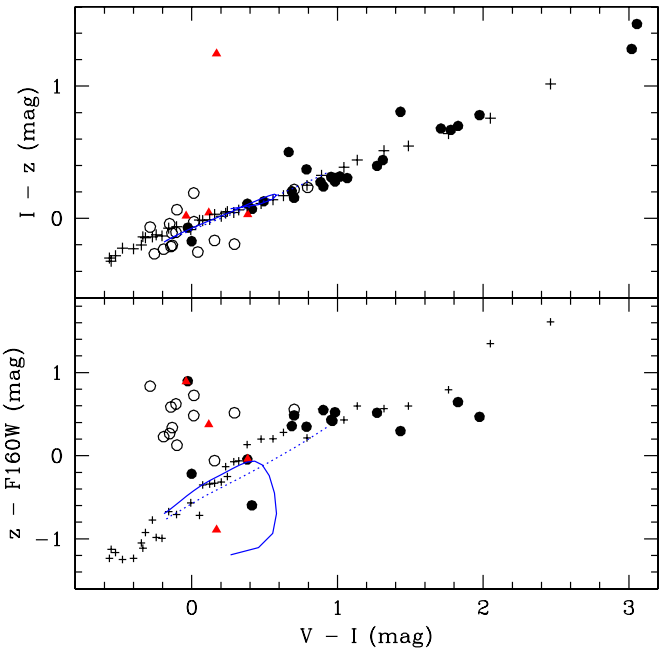

Figure 8. Optical and infrared color–color diagrams for the 46 unresolved source candidates in the UDF. Filled and open circles show bright ($I < 27$ mag) and faint ($I > 27$ mag) objects, respectively. Triangles mark the spectroscopically confirmed quasars, and the plus symbols show the synthetic colors of Pickles (1998) stellar templates for O5 to M6 type dwarfs. Colors for 3000–10,000 K pure H (solid lines) and 3500–10,000 K pure He (dotted lines) atmosphere white dwarf models are also shown.

(A color version of this figure is available in the online journal.)

Figure 9 shows the optical and infrared SEDs and best-fit stellar templates for UDF 7113 and 8081. UDF 7113 has colors best-matched by a K7 star, while UDF 8081 has colors that are similar to spectroscopically confirmed quasars. Even though the optical portion of UDF 8081's SED is best-matched by an A2 type star, its infrared SED is too red for an A type star or a white dwarf. Hence, UDF 8081 is most likely an extragalactic object. UDF 9006 is potentially interesting; its sharpness parameter of 0.18 and its radial profile is similar to the unresolved sources in the UDF. However, UDF 9006 also has an infrared SED that is too red for a blue main-sequence star or a white dwarf. UDF 7113 is the only target fainter than $I = 27$ mag that has a radial profile and an optical and infrared SED consistent with stars.

5. DISCUSSION

5.1. Late-type Stars

There are 25 stars in the UDF down to $I = 27$ mag, including 24 K0 or later type stars and 1 F5 type star. Fainter than this limit, UDF 7113 ($I = 27.67$ mag) is the only source that looks like a star, bringing the total number of stars in the UDF to 26. To estimate photometric distances, we adopt the absolute magnitude (M_V) for each spectral type from Pickles (1998), and use it to calculate synthetic absolute magnitudes in the ACS F606W filter (M_{F606W}). We calculated photometric distances for all of the objects in our sample using the synthetic M_{F606W} and the observed V_{F606W} magnitudes. Spectral types from our SED fitting procedure, proper motions, absolute magnitudes, distances, and tangential velocities are given in Table 1. The photometric errors for the UDF point sources are relatively small; the resulting errors in the estimated distances are also

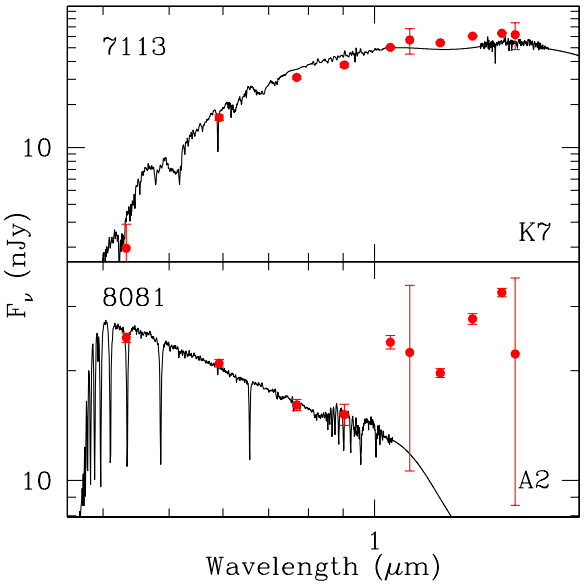

Figure 9. Optical and infrared SEDs and the best-fitting main-sequence star templates (Pickles 1998) for the faint ($I > 27$ mag) unresolved sources.

(A color version of this figure is available in the online journal.)

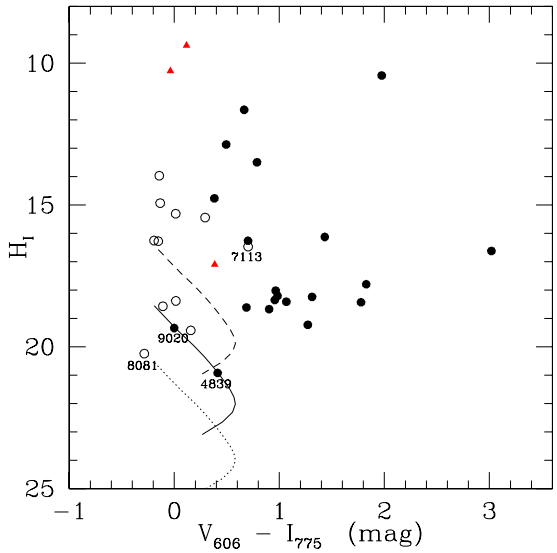

Figure 10. Reduced proper motion diagram for the unresolved source candidates in the UDF. Filled and open circles show bright ($I < 27$ mag) and faint ($I > 27$ mag) sources, respectively. Triangles mark the spectroscopically confirmed quasars. Dashed, solid, and dotted lines show the cooling sequences for disk ($V_{\rm tan} = 30$ km s^{-1}), thick disk (80 km s^{-1}), and halo (200 km s^{-1}) white dwarfs.

(A color version of this figure is available in the online journal.)

very small. However, if the assigned spectral types are wrong by 1 index, the absolute magnitudes could be wrong by as much as 1 mag.

The stellar templates we use have approximately solar metallicity. Therefore, the distances to the metal-poor halo objects, which will be intrinsically fainter for the same spectral type, are over-estimated by our SED fitting method. To verify the effect of different metallicities, we use synthetic spectra from a PHOENIX model atmosphere grid (Brott & Hauschildt 2005) for stars with $T_{\rm eff} = 2000$–10,000 K, [Fe/H] $= 0, -2$, and $\log(g) = 4.5$. The best-fit temperature for the halo metallicity models are on average 300 K cooler (see the last two columns in Table 1). This difference in temperature implies that the distances and tangential velocities presented in Table 1 are likely overestimated for metal-poor stars by a factor of $\geqslant 2$ (Bressan et al. 2012). Despite these potential systematic errors, available kinematic data is sufficient to identify disk and halo stars and white dwarfs.

The majority of the K0 and later type dwarf stars are consistent with being a late-type star in the disk or halo of the Galaxy. Out of the 25 bright stars, 23 are at distances in the range 1–62 kpc. UDF 7113 is consistent with a K7 dwarf at a distance of $\sim$100 kpc and $V_{\rm tan} = 340$ km s^{-1}. Even though there are several objects with relatively large $V_{\rm tan}$, given the uncertainties due to unknown metallicities and the errors in our proper motion measurements (on the order of 1.4 mas yr^{-1}), these tangential velocity estimates are consistent with halo membership within the errors.

We used the analytical form of the density profile for the Galactic disk and the halo (Gilmore et al. 1990; von Hippel & Bothun 1990) to calculate the expected number of stars in the UDF. Assuming a local normalization of 0.11 $M_\odot$ pc^{-3} (Pham 1997), we expect to find 3 thin disk, 6 thick disk, and 20 halo stars in the UDF. Reid & Majewski (1993) star count models predict 4 thin disk, 8 thick disk, and 19 halo stars, whereas the Besançon galaxy model predicts 32 stars down to $I = 27$ mag, including two white dwarfs. Given the small field of view of the UDF and the small number statistics, the observed number of stars (25–26) and the predictions of star count models (29–32) are in good agreement.

5.2. White Dwarfs

Pirzkal et al. (2005) identified four white dwarf candidates in the UDF, objects 4322, 4839, 7768, and 9020. Our analysis shows that one of these objects, UDF 4322, is resolved, and therefore almost certainly an extragalactic object. Unfortunately, no proper motion information is available for UDF 4322 to support this argument. However, its infrared colors and SED are not like any known white dwarf, and they are similar to quasars.

Reduced proper motion diagrams provide a clean method for identifying white dwarfs in large surveys (Kilic et al. 2006, 2010). Figure 10 shows a reduced proper motion diagram for the unresolved source candidates in the UDF along with evolutionary sequences for disk and halo white dwarfs from the models of Tremblay & Bergeron (2009). These models include the collision-induced absorption (CIA) due to molecular hydrogen (Borysow et al. 1997) and the red-wing of the Ly α opacity (Kowalski & Saumon 2006). The model colors turn to the blue around 4000 K due to the CIA. There are two sources, UDF 4839 and 9020, with $I < 27$ mag that are consistent with thick disk white dwarfs.

As a main-sequence star, UDF 4839 would have a tangential velocity well in excess of 5000 km s^{-1} at a distance of 100 kpc. Similarly, UDF 9020 would have a tangential velocity well in excess of 6000 km s^{-1} at a distance of 443 kpc. Obviously, both of these point sources must be white dwarfs. The fourth white dwarf candidate, UDF 7768, is consistent with a K7 type main-sequence star at 32 kpc and its reduced proper motion and colors are similar to the other main-sequence stars in the UDF. Hence, UDF 7768 is most likely a main-sequence star. This leaves us with two white dwarf candidates brighter than $I = 27$ mag, UDF 4839 and 9020.

Figure 11 shows the SEDs and the best-fit pure-H (solid line) and pure-He (dashed line) white dwarf model atmospheres for

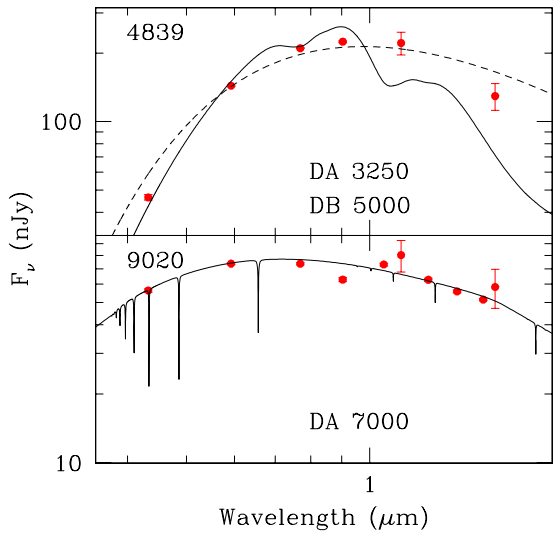

Figure 11. Optical and infrared SEDs and the best-fitting pure H (solid lines) and pure He (dashed lines) white dwarf models for UDF 4839 and 9020.
(A color version of this figure is available in the online journal.)

UDF 4839 and 9020. Thanks to the infrared photometry from the UDF12 program and Coe et al. (2006), for the first time, we are able to compare the SEDs of young and old white dwarfs simultaneously and find the best-fit solutions for the UDF white dwarf candidates.

UDF 4839 is best fit by a 5000 K pure-helium atmosphere white dwarf at a distance of 1.6 kpc and $V_{\rm tan} = 90$ km s^{-1}. Its infrared photometry shows a slight flux deficit that may be the signature of the CIA due to molecular hydrogen. However, the infrared photometry is not precise enough to confirm hydrogen in the atmosphere. The best-fit hydrogen atmosphere model has $T_{\rm eff} = 3250$ K, $d = 0.6$ kpc, and $V_{\rm tan} = 35$ km s^{-1}. Regardless of the composition, UDF 4839 is clearly a 6–10 Gyr old thick disk white dwarf within 0.6–1.6 kpc of the Sun.

UDF 9020 is best-fit by a 7000 K pure-hydrogen atmosphere white dwarf model at a distance of 4.5 kpc and $V_{\rm tan} = 70$ km s^{-1}. The best-fit pure helium atmosphere model also has $T_{\rm eff} = 7000$ K. Regardless of the composition, UDF 9020 is a $\sim$1.5 Gyr old thick disk white dwarf within 4.5 kpc of the Sun. Unfortunately, we do not have any information on the masses of these white dwarfs. Bergeron et al. (2005) emphasized the importance of precise mass determinations in order to determine the total stellar ages of the white dwarfs and classify their memberships accordingly. If UDF 9020 is a $\approx$0.5 $M_\odot$ white dwarf, its total age would be $\sim$12 Gyr, consistent with the thick disk population. In summary, both UDF 4839 and 9020 have PSFs consistent with unresolved objects, they display proper motion, and their colors are consistent with relatively old white dwarfs in the Galactic thick disk.

Based on our proper motion measurements and the reduced proper motion diagram presented in Figure 10, UDF 8081 is the only object in our sample that would be consistent with a white dwarf in the halo. However, its SED demonstrates that UDF 8081 is clearly not a white dwarf. Therefore, we do not find any white dwarfs in the UDF with halo kinematics.

5.2.1. Space Density of White Dwarfs

Pirzkal et al. (2005) calculated the white dwarf space density in the UDF using a simple $1/V_{\rm max}$ analysis (Schmidt 1968) and found a local density of between 3.5×10^{-5} and 1.1×10^{-2} stars pc^{-3}. We perform a similar analysis using the two white dwarfs in the UDF. For a limiting magnitude of $I = 27$ mag and using the best-fit white dwarf models, we estimate a local density of 1.3×10^{-4} pc^{-3} for the thick disk white dwarfs. If UDF 4839 is a very cool DA (Figure 11) at a distance of 0.6 kpc, the local density of thick disk white dwarfs would increase to 1.7×10^{-3} pc^{-3}. Sion et al. (2009) estimate a local white dwarf space density of $4.9 \pm 0.5 \times 10^{-3}$ pc^{-3} using the 20 pc volume-limited sample. The thick disk white dwarfs in the UDF correspond to 3%–35% of the local space density of white dwarfs. This is in good agreement with the normalization for thick disk white dwarfs (Reid 2005; Rowell & Hambly 2011).

The Besançon Galaxy models predict two white dwarfs with $I \leqslant 27$ mag. Both are predicted to be thick disk white dwarfs with $d = 1.4$–2.2 kpc and $V_{\rm tan} = 25$–45 km s^{-1}. These are consistent with the observed properties of UDF 4839 and 9020, the two white dwarfs brighter than $I = 27$ mag in the UDF. The Besançon model predicts two additional white dwarfs with $I = 27$–29 mag, including a halo white dwarf with $V_{\rm tan} = 235$ km s^{-1}. The only faint ($I > 27$ mag) unresolved source in the UDF with a star-like SED is UDF 7113. The best-fit stellar template for UDF 7113 is a K7 main-sequence star. If UDF 7113 is a white dwarf, its SED would be best-matched by a 3750 K pure helium-atmosphere white dwarf at a distance of 2.1 kpc and $V_{\rm tan} = 6$ km s^{-1}. Obviously, UDF 7113 is not a halo white dwarf. Finding zero halo white dwarfs, when the expected number is one, is not surprising. Hence, this analysis shows that the observed number of white dwarfs in the UDF does not require additions to the standard Galactic models.

6. CONCLUSIONS

A careful analysis of the radial profiles, proper motions, and the SEDs of point-like sources in the UDF revealed 25 stars brighter than $I = 27$ mag and one more likely star (UDF 7113) with $I = 27.67$ mag. Combining the optical photometry with the 1.0–1.6 μm photometry from the UDF12 program enabled us to fit the SEDs of each star and constrain their spectral types, distances, and tangential velocities. Out of the 26 stars, 12 have significant ($>3\sigma$) proper motions, and 24 are consistent with late-type K-M dwarfs in the disk or halo of the Galaxy. This analysis revealed two stars that are too faint to be main-sequence stars, UDF 4839 and 9020. These are clearly thick disk white dwarfs at distances of 0.6–4.5 kpc and $V_{\rm tan} = 35$–90 km s^{-1}.

All three deep fields observed by *HST*, Hubble Deep Field North, South, and the UDF, have two white dwarf candidates brighter than $I = 27$ mag (Kilic et al. 2004, 2005, and this study). A comparison of the observed number of white dwarfs in these deep pencil-beam surveys with model predictions shows that the observed white dwarf population in the *HST* deep fields do not require any additions to the standard Galactic models.

This material is based upon work supported by the National Aeronautics and Space Administration under grant NNX11AF34G issued through the Office of Space Science.

REFERENCES

Alcock, C., Allsman, R. A., Alves, D. R., et al. 2000, ApJ, 542, 281
Beckwith, S. V. W. 2005, yCat, 2258, 0
Bergeron, P., Ruiz, M. T., Hamuy, M., et al. 2005, ApJ, 625, 838
Bergeron, P., Wesemael, F., Dufour, P., et al. 2011, ApJ, 737, 28
Bertin, E., & Arnouts, S. 1996, A&AS, 117, 393
Borysow, A., Jorgensen, U. G., & Zheng, C. 1997, A&A, 324, 185

Bressan, A., Marigo, P., Girardi, L., et al. 2012, MNRAS, 427, 127
Brott, I., & Hauschildt, P. H. 2005, in The Three-dimensional Universe with Gaia, ed. C. Turon, K. S. O'Flaherty, & M. A. C. Perryman (ESA SP-576; Noordwijk: ESA), 565
Calchi Novati, S. 2010, GReGr, 42, 2101
Casertano, S., de Mello, D., Dickinson, M., et al. 2000, AJ, 120, 2747
Coe, D., Benítez, N., Sánchez, S. F., et al. 2006, AJ, 132, 926
Ellis, R. S., McLure, R. J., Dunlop, J. S., et al. 2013, ApJL, 763, L7
Gilmore, G., King, I. R., van der Kruit, P. C., & Buser, R. 1990, Sci, 250, 703
Ibata, R. A., Richer, H. B., Gilliland, R. L., & Scott, D. 1999, ApJL, 524, L95
Kilic, M., Leggett, S. K., Tremblay, P.-E., et al. 2010, ApJS, 190, 77
Kilic, M., Mendez, R. A., von Hippel, T., & Winget, D. E. 2005, ApJ, 633, 1126
Kilic, M., Munn, J. A., Harris, H. C., et al. 2006, AJ, 131, 582
Kilic, M., von Hippel, T., Mendez, R. A., & Winget, D. E. 2004, ApJ, 609, 766
Koekemoer, A. M., Ellis, R. S., McLure, R. J., et al. 2012, ApJS, submitted (arXiv:1212.1448)
Kowalski, P. M., & Saumon, D. 2006, ApJL, 651, L137
Mahmud, N., & Anderson, J. 2008, PASP, 120, 907
Méndez, R. A., & Minniti, D. 2000, ApJ, 529, 911
Pham, H.-A. 1997, in *Hipparcos*—Venice '97, ed. R. M. Bonnet et al. (ESA SP-402; Noordwijk: ESA), 559
Pickles, A. J. 1998, PASP, 110, 863
Pirzkal, N., Sahu, K. C., Burgasser, A., et al. 2005, ApJ, 622, 319
Pirzkal, N., Xu, C., Malhotra, S., et al. 2004, ApJS, 154, 501
Reid, I. N. 2005, ARA&A, 43, 247
Reid, N., & Majewski, S. R. 1993, ApJ, 409, 635
Rowell, N., & Hambly, N. C. 2011, MNRAS, 417, 93
Schmidt, M. 1968, ApJ, 151, 393
Sion, E. M., Holberg, J. B., Oswalt, T. D., McCook, G. P., & Wasatonic, R. 2009, AJ, 138, 1681
Tremblay, P.-E., & Bergeron, P. 2009, ApJ, 696, 1755
von Hippel, T., & Bothun, G. 1990, AJ, 100, 403
Williams, R. E., Blacker, B., Dickinson, M., et al. 1996, AJ, 112, 1335